

Article

Microstructure, Mechanical Properties and Deformation Behavior of Fe-28.7Mn-10.2Al-1.06C High Specific Strength Steel

Liang Ma ¹, Zhengyou Tang ^{1,2,*}, Zeyu You ¹, Guofu Guan ¹, Hua Ding ^{1,2} and Devesh Misra ³

¹ School of Materials Science and Engineering, Northeastern University, Shenyang 110819, China; 15040120855@163.com (L.M.); zeyuyou@163.com (Z.Y.); ggf2467065710@163.com (G.G.); cc18640145348@163.com (H.D.)

² Key Laboratory of Lightweight Structural Materials, Northeastern University, Shenyang 110819, China

³ Laboratory for Excellence in Advanced Steel Research, Department of Metallurgical, Materials and Biomedical Engineering, University of Texas at El Paso, El Paso, TX 79968, USA; rdkmisra@163.com

* Correspondence: tangzy@smm.neu.edu.cn; Tel.: +86-13478183256

Abstract: The microstructure, properties and deformation behavior of Fe-28.7Mn-10.2Al-1.06C high specific strength steel were studied. The results showed that the density of experimental steel is about 6.59 g/cm³ and the microstructure is austenite. With the increase in the annealing temperature, the tensile strength decreases and the elongation increases. When the annealing temperature is 950 °C, the strength-plastic product of the experimental steel is 54.82 GPa%, and the specific strength is 1.48 × 10⁵ N·m/kg. Compared with 20Mn2CrNb high strength automobile steel, the specific strength of laboratory steel is increased by more than 20%. The deformation behavior of experimental steel is mainly: At the low strain, spacing of slip surface decreases; at high strain, dislocation walls and micro-strips are formed, and the austenite grains are segmented, increasing the dislocation density and starting more secondary slips.



Citation: Ma, L.; Tang, Z.; You, Z.; Guan, G.; Ding, H.; Misra, D. Microstructure, Mechanical Properties and Deformation Behavior of Fe-28.7Mn-10.2Al-1.06C High Specific Strength Steel. *Metals* **2022**, *12*, 602. <https://doi.org/10.3390/met12040602>

Academic Editor: Marcello Cabibbo

Received: 9 March 2022

Accepted: 29 March 2022

Published: 31 March 2022

Publisher's Note: MDPI stays neutral with regard to jurisdictional claims in published maps and institutional affiliations.



Copyright: © 2022 by the authors. Licensee MDPI, Basel, Switzerland. This article is an open access article distributed under the terms and conditions of the Creative Commons Attribution (CC BY) license (<https://creativecommons.org/licenses/by/4.0/>).

Keywords: high specific strength steel; annealing temperature; mechanical properties; deformation behavior

1. Introduction

At present, the lightweight automobile has become the trend of automobile development in the world, and it has great strategic significance for the development of the automobile industry and energy conservation and emission reduction [1]. The advanced high strength for automobiles mainly realizes the gradual thinning of steel plate thickness and the gradual reduction in body weight through good strength and plasticity matching. However, the design of automobile components still needs to meet certain stiffness requirements, and its thickness cannot be reduced unlimitedly with the increase in steel plate strength, which puts forward higher requirements for the specific strength (the ratio of strength to density) and plasticity of materials [2–4].

Fe-Mn-Al-C system is a promising, highly specific strength steel with excellent mechanical properties (yield strength: 0.4~1.0 GPa; tensile strength: 0.6~2.0 GPa; and elongation: 30~100%) and low specific weight (1.3% density reduction per 1wt% Al addition) [5–9]. The addition of Mn increases the face-centered cubic lattice parameters, and the very high Mn and C contents stabilize the austenite, so it can tolerate the addition of Al up to 10% without damaging the face-centered cubic (FCC) structure [10,11].

In recent years, researchers from various countries have studied the microstructure, mechanical properties, and deformation mechanism of Fe-Mn-Al-C steel. Kim et al. [12] established a thermodynamic database of Fe-Mn-Al-C steel. C Zhao et al. [13] studied the effect of annealing temperature on the microstructure and properties of Fe-Mn-Al-C steel, and found that the content of austenite in the experimental steel determines the final

elongation. Yoo et al. [14] found that the steel with Fe-28Mn-9Al-0.8C composition had plane slip during deformation, and proposed the mechanism of plastic deformation caused by micro-strips. Frommeyer et al. [15] found that nanometer-sized ordered phases can be obtained for Fe-26/28Mn-10/12Al-1.0/1.2C steel through microstructure adjustment, and shear bands are formed during unidirectional continuous tensile deformation, resulting in shear band induced plasticity. Welsch et al. [16] studied the strain hardening mechanism of Fe-30.4Mn-8Al-1.2C steel and found that dynamic slip band refinement is the main strain hardening mechanism.

At present, the specific strength of Fe-Mn-Al-C steel is mainly improved by adding Al element. However, with the addition of a large amount of Al element, the strong-plastic product will decrease [4,17]. The effect of Al element on mechanical properties is not clear. Moreover, Fe-Mn-Al-C steel has high alloy content and strict heat treatment process which need more detailed research. At the same time, the deformation mechanism of Fe-Mn-Al-C series steel is still unclear, and the deformation behavior of Fe-Mn-Al-C steel needs experimental verification and in-depth discussion. In this study, a highly specific strength steel (Fe-28.7Mn-10.2Al-1.06C) was developed by composition optimization, and the microstructure and properties of the experimental steel were optimized by controlling the annealing process. The deformation behavior of the experimental steel after annealing was discussed in depth. It provides a theoretical basis for the composition design, performance optimization, and discussion of deformation mechanism of Fe-Mn-Al-C high specific strength steel.

2. Materials and Methods

A 50 kg ingot with a composition of Fe-28.7Mn-10.2Al-1.06C in weight percent was prepared by induction melting. Hot-forged into a slab with a sectional dimension of 100 mm × 30 mm. The mass of the experimental steel was weighed by an electronic analytical balance, the volume of the experimental steel was measured by the drainage method, and the density of the experimental steel was calculated to be 6.59 g/cm³.

After homogenization at 1200 °C for 2 h, the slab was hot-rolled to the plates of 3 mm in thickness. Subsequently, the hot-rolled plates were solid-solution treated at 1000 °C for 1 h, followed by water quenching (WQ) to room temperature. The hot-rolled plates were rolled at room temperature to make 1 mm-thick sheets. The cold-rolled steel sheets annealed at 900, 950, 1000, 1050, and 1100 °C for 15 min, followed by cooling in water.

Microstructural examination was carried out using an optical microscope (OM, OLYMPUS DSX500, Tokyo, Japan), and a transmission electron microscope (TEM, Tecnai G² 20, operated at 200 kV, FEI, Hillsboro, OR, USA). Specimens for OM observations were electro-polished, and then etched using a solution of 1ml hydrochloric acid, 100 mL methanol, and 4 g picric acid. Thin foils for TEM observation were electro-polished in a mixed solution of 90% ethanol and 10% perchloric acid using a twin-jet polisher. TEM analysis was performed at an acceleration voltage of 200 kV.

Constituent phases in annealed specimens were identified by X-ray diffraction (XRD, Rigaku, D/Max2250/PC, Rigaku Corporation, Tokyo, Japan). The scan angle was 40~100° and the scan rate was 2°/min. ASTM E8 sub-sized tensile specimens with a gauge portion of 6 mm in width and 25 mm in length were machined from the annealed plates along the rolling direction. Tensile tests were carried out using a universal testing machine (SANSCMT5000, MTS, Eden Prairie, MN, USA) at an initial strain rate of 1 × 10⁻³/s at room temperature. Three samples were taken from each annealing process to determine mechanical properties. Observation of fracture morphology after stretching by scanning electron microscope (SEM, Supra, SSX-550, Shimadzu, Tokyo, Japan).

3. Results and Discussion

3.1. Microstructure

Figure 1 shows the metallographic structure and XRD pattern of the cold-rolled experimental steel. It can be seen from the figure that the microstructure of the cold-rolled experimental steel is austenite.

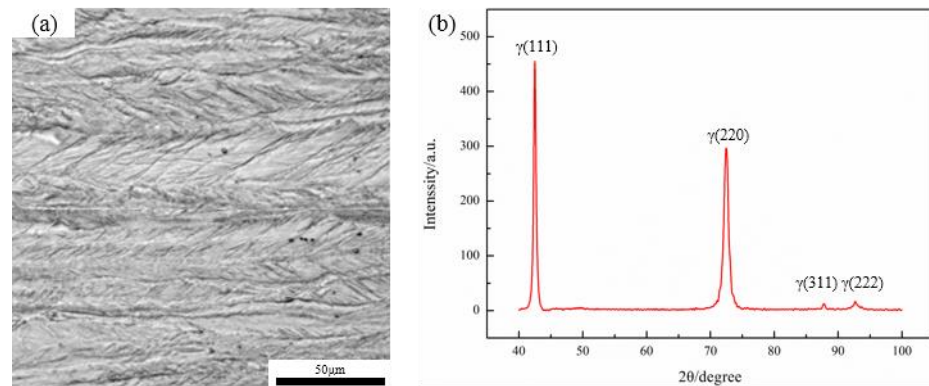


Figure 1. (a) Microstructure of Cold Rolled Experimental Steel; (b) XRD of Cold Rolled Experimental Steel.

Figure 2 is the XRD diffraction pattern of cold rolled experimental steel annealed at 900~1100 °C for 15 min and TEM morphology and diffraction spots. The test results show that the experimental steel consists of austenite and trace amount of κ -carbide.

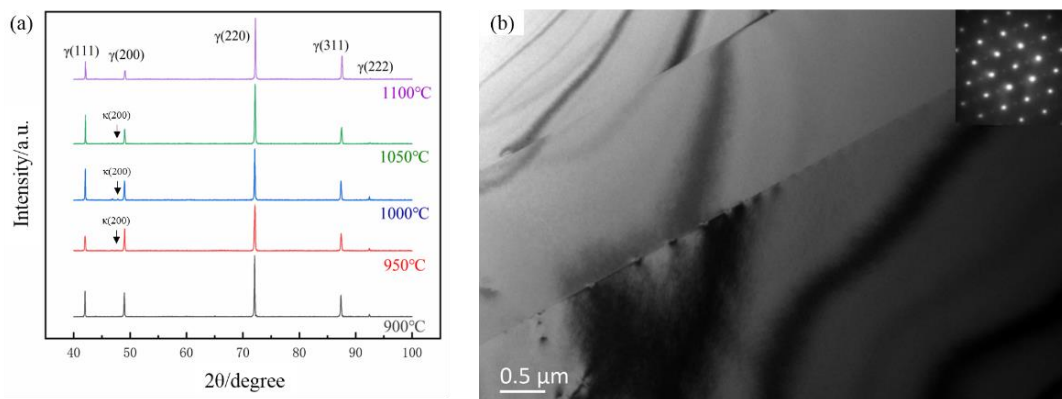


Figure 2. (a) XRD patterns of experimental steel annealed at different temperatures for 15 min; (b) 950 °C TEM Morphology and diffraction spots.

Figure 3 shows the microstructure of the cold-rolled experimental steel annealed at 900~1100 °C for 15 min. Table 1 shows the grain size of the experimental steel at different annealing temperatures. After annealing at 900 °C, the cold-rolled microstructure in the experimental steel basically disappears. At this time, there are a large number of austenite grains in the microstructure. The grain size is about 22 μm , and the shape is irregularly distributed. A small amount of twins appear in the austenite grains. When the annealing temperature reaches 1100 °C, the austenite grains continue to grow into equiaxed grains, and the grain size is about 156 μm . With the gradual increase in annealing temperature, the grain size increases, which is due to the increase in temperature. The diffusion ability of each element increases, and the migration rate of grain boundary increases. At the same time, the growth rate of annealing twins formed in some grains is greater than the migration rate of grain interface, so that it runs through the entire austenite grain [18].

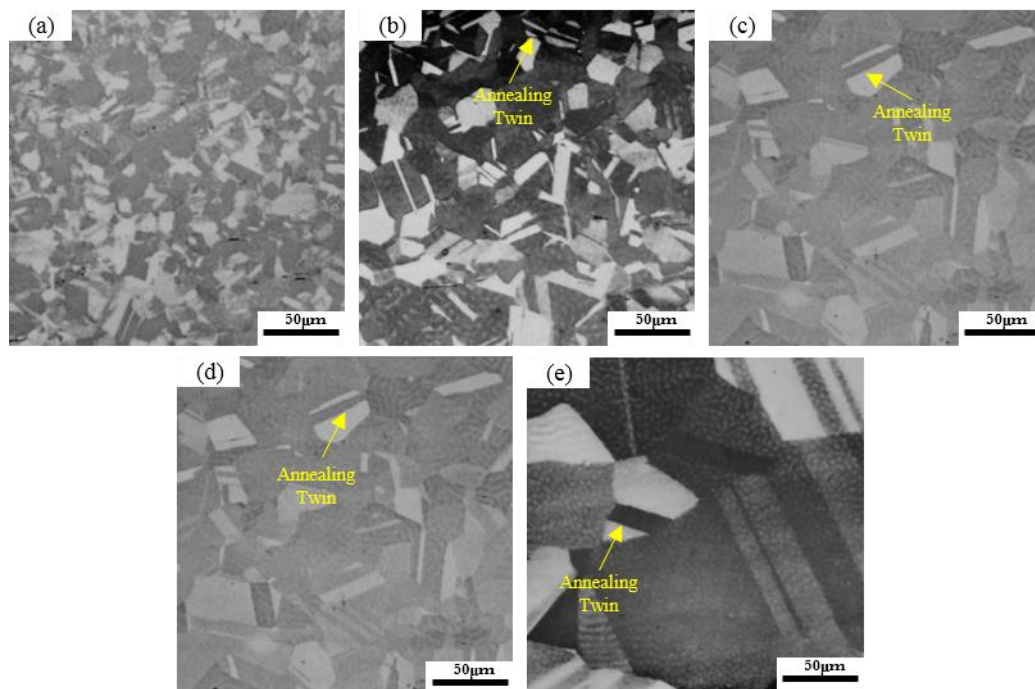


Figure 3. OM morphology of experimental steel annealed at different temperatures for 15 min. (a) 900 °C; (b) 950 °C; (c) 1000 °C; (d) 1050 °C; and (e) 1100 °C.

Table 1. Grain size at different annealing temperature.

900 °C	950 °C	1000 °C	1050 °C	1100 °C
22 ± 2 μm	30 ± 5 μm	42 ± 4 μm	81 ± 6 μm	156 ± 13 μm

3.2. Mechanical Properties

Fe-Mn-Al-C steel can achieve the excellent combination of strength and ductility. Figure 4 shows the engineering stress–strain curves of the experimental steel under different annealing processes. The alloy exhibits continuous yield during the tensile deformation without obvious yield platform. The mechanical properties of the experimental steel annealed at different temperatures are shown in Table 2. Under the annealing temperature of 950 °C and holding time of 15 min, the tensile strength of the experimental steel was 977.2 MPa, the elongation was 56.1%, and the product of strength and plasticity was as high as 54.82 GPa%. The density was 6.59 g/cm³ and the specific strength was 1.48 × 10⁵ N·m/kg measured by the drainage method. Fe-27Mn-8Al-1.6C is the same as the type of alloying elements added in the experimental steel, the annealed structures of both are composed of austenite and a small amount of carbides. The tensile strength of Fe-27Mn-8Al-1.6C is 1266 MPa, the elongation is 34%, and the strong-plastic product is 43.1GPa% [19]. Compared with Fe-27Mn-8Al-1.6C, the strength-plastic product of the experimental steel is increased by 11.7 GPa%. Compared with 20Mn2CrNb [20] high strength automobile steel with tensile strength of 905 MPa and density of 7.8 g/cm³, the specific strength of the experimental steel is increased by more than 20%.

With the increase in annealing temperature, the tensile strength of the experimental steel decreases and the elongation increases. The reason for this situation is that, after annealing treatment, the grains of the experimental steel grow up in varying degrees. Figure 5 is the relationship between yield strength and $d^{-1/2}$, and fitting it with the Hall–Petch equation. According to the Hall–Petch equation ($\sigma_s = \sigma_0 + Kd^{-1/2}$) it can be seen that with the increase in grain size, the yield strength decreases. The grain boundary area per unit volume decreases, and the hindrance of grain boundary on dislocation slip during plastic deformation leads to the decrease in strength. At the same time, due to

the grain growth, the number of dislocations in the dislocation plug cluster at the grain front increases. Under the same external load, it will cause greater stress concentration. Stress concentration can make the sliding system near the grain start in advance, which is conducive to coordinating deformation, increasing the uniformity of plastic deformation, and improving the elongation.

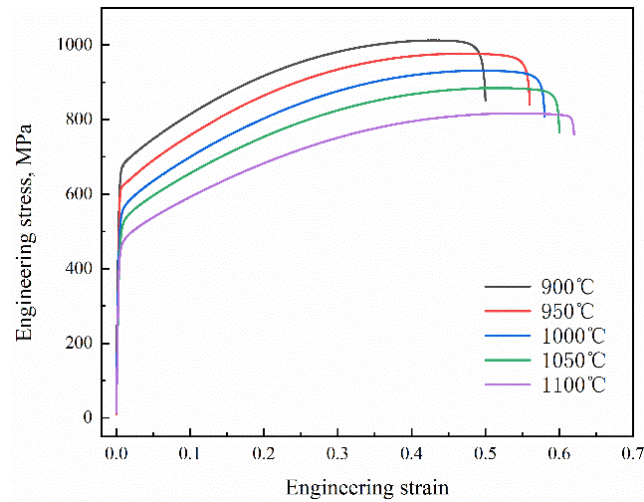


Figure 4. Engineering stress–strain curves of experimental steel under different annealing conditions.

Table 2. Mechanical properties of experimental steel under different annealing conditions.

Temperature	YS/MPa	UTS/MPa	TEL	PSE/(GPa%)	Specific Strength/ N·m/kg
900 °C	680.7 ± 5.3	1012.4 ± 6.5	50.2 ± 0.2%	50.82	1.54 × 10 ⁵
950 °C	619.2 ± 3.1	977.2 ± 4.2	56.1 ± 0.3%	54.82	1.48 × 10 ⁵
1000 °C	559.4 ± 4.7	931.6 ± 4.1	58.3 ± 0.4%	54.31	1.41 × 10 ⁵
1050 °C	525.1 ± 5.4	884.6 ± 6.3	60.4 ± 0.2%	53.43	1.34 × 10 ⁵
1100 °C	473.6 ± 1.6	816.7 ± 0.9	62.1 ± 0.5%	50.72	1.24 × 10 ⁵

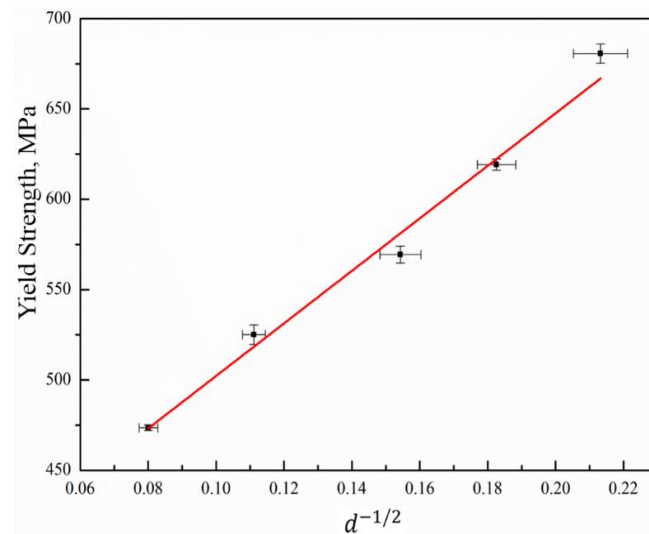


Figure 5. Relationship between yield strength and $d^{-1/2}$.

In addition, there are a large number of complete and incomplete annealing twins in the grains of the experimental steel after annealing treatment, which are generated during the recrystallization growth process. These twin boundaries act as subgrain boundaries to increase the total area of grain boundaries in the structure, so that the original coarse

austenite grains are refined, and the twin boundaries hinder dislocation slip, playing the role of grain boundary strengthening. At the same time, the content of alloying elements in the experimental steel is relatively high, so the effect of solid solution strengthening is more obvious. In particular, C element can play a role in interstitial solid solution strengthening, and the strengthening effect can reach 187~300 MPa/wt% [21]. The test steel still has high strength under the premise of good elongation [22].

3.3. Deformation Behavior

Figure 6a is the true stress–strain curve and work hardening rate curve of the experimental steel annealed at different temperatures. Taking 950 °C as an example, it can be divided into three stages: I—Continuous decrease in work hardening rate at initial stage of plastic deformation: when the true strain was 0.0167, the work hardening rate decreased to 2483.02 MPa; II—Deformation hardening stage: at this stage, with the increase in true strain, the work hardening rate declined slowly; and III—Work hardening rate decay stage: when the true strain >0.3321, the work hardening rate decreases rapidly until fracture. Figure 6b is the tensile fracture morphology of the experimental steel annealed at 950 °C for 15 min. The dimples and tearing edges with different sizes can be observed in the fracture morphology. The characteristic results of the fracture morphology are consistent with the tensile properties of Figure 4, which shows the characteristics of ductile fracture.

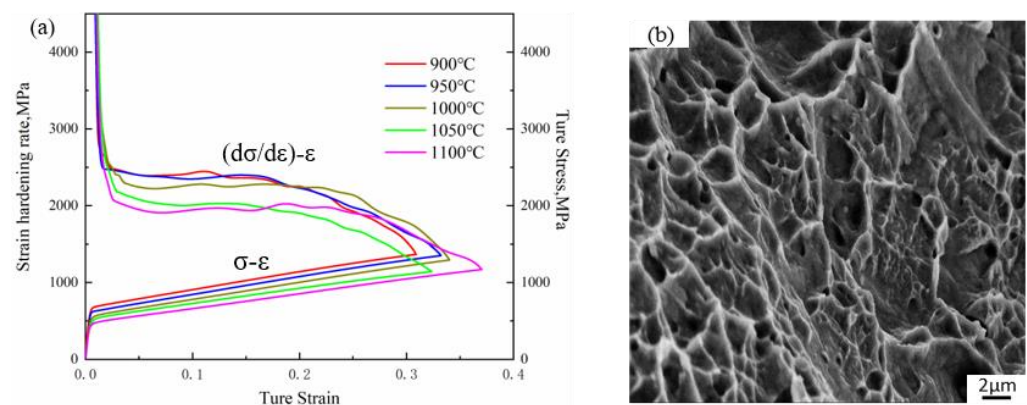


Figure 6. (a) True stress–strain curve and work hardening rate curve; (b) 950 °C fracture morphology.

The addition of Al significantly improves the stacking fault energy of austenitic steel, thereby affecting the deformation behavior of austenitic steel. The experimental steel has higher Al content, which also makes it have high stacking fault energy, which can reach $78.2 \text{ MJ}\cdot\text{m}^{-2}$; the TRIP and TWIP effects are also greatly inhibited [23–25]. However, it still has high work hardening ability, which is closely related to the unexpected plane slip mode of dislocation. This mode reduces the dynamic recovery in the deformation process, and transfers the deformation stage to high strain, thereby enhancing the storage capacity of dislocation [16,26].

Figure 7 shows the TEM images of tensile fracture at different annealing temperatures. It can be seen from the graph that slip is carried out on {111} plane, the structure after fracture is dominated by micro-strip and dislocation wall. As the annealing temperature increases, the grains grow and the total grain boundary area decreases, the yield strength decreases, and slip is more likely to occur, resulting in an increase in the micro-strip density, and the micro-strip with different orientations can effectively coordinate deformation, so that the material has higher elongation. At the same time, as the high-density dislocation wall can prevent the dislocation movement, a large number of micro-strip structures divide the austenite grain. After dividing the grain, the micro-strip structure plays the role of sub-grain boundary, which hinders the dislocation slip as an immobile barrier and improves the strength of the material [27].

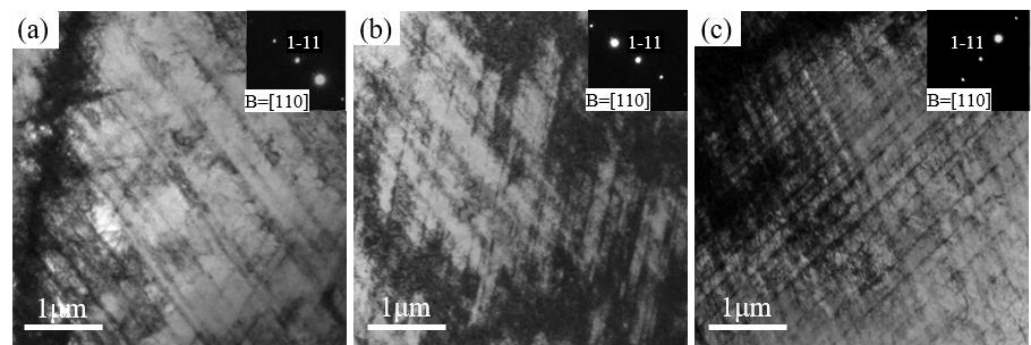


Figure 7. TEM images of the experimental steel after fracture at different annealing temperatures. (a) 900 °C; (b) 950 °C; and (c) 1000 °C.

In order to further study the deformation behavior and deformation process of the experimental steel, tensile tests with different deformations were carried out on the 950 °C annealed experimental steel. It can be seen from Figure 8 that slip occurs on {111} plane. Figure 8a,b is the TEM image of the experimental steel with deformation of 5%. Through the image, it can be observed that the dislocation structure of the experimental steel at low deformation is plane slip dislocation, and some basic dislocation structures can also be observed: dislocation pair (marked at A in Figure 8a), pressure lever dislocation (marked at B in Figure 8b), and dislocation pile-up (marked at C in Figure 8b). Due to the three-dimensional immovability of pressure lever dislocations, it plays an important role in the work hardening of face-centered cubic metals. In order to quantitatively analyze the structural distribution of plane dislocations, the width and spacing of plane slip dislocations in grains were measured. The average width and spacing of plane dislocations are 156 nm and 328 nm. Figure 8c,d is the TEM image of the experimental steel with 10% deformation. It can be observed that with the increase in deformation, a large number of slip trajectories appear, the dislocation density of slip band increases, the average width and average spacing size of plane slip dislocations decrease, which are 93 nm and 186 nm, respectively.

Figure 8e is the TEM image of the experimental steel with 20% deformation. With the further increase in strain, the applied load increases gradually, resulting in more dense plane slip dislocations. The average width and spacing of plane slip dislocations are further reduced to 58 nm and 131 nm, respectively, which greatly increase the dislocation density. The multi-system slip characteristics produced by two non-coplanar slip systems appear, and low density dislocation tangles appear in the intersection area of the main slip band and the secondary slip band (marked at D and E in Figure 8e). This is due to the interaction between dislocations, easily leading to defects and dislocation concentration to reach the dislocation slip critical stress and produce more dislocations. Figure 8f is a TEM image of the experimental steel with a deformation of 50%. As the deformation increases to 50%, it can be observed that parallel high-density dislocation walls appear in addition to the multi-system slip characteristics, and these high-density dislocation walls and areas sandwiched between them are called micro-strips (marked at F in Figure 8f).

In the initial deformation stage, under the action of the finite slip system, the strain is accommodated by reducing the spacing of the slip surface in the Taylor lattice. At this time, the dislocation distribution around the slip surface is uniformly distributed and the plane is orderly. In this case, due to their alternation and mutual screening, the stored energy is reduced, and the dislocation density is increasing, resulting in a slow decrease in the strain hardening rate. When the deformation is higher than 40%, more dislocation walls and micro-strips are formed, and the grains subdivided by their intersections are dominant. The more the Taylor lattice rotates to adapt to strain, the more dislocation walls and micro-strips are formed, which provide another strain adaptation process under high strain. In addition to strain hardening, grain refinement is also an additional strengthening factor at high deformation, so that the experimental steel has good strength and ductility [15,28,29].

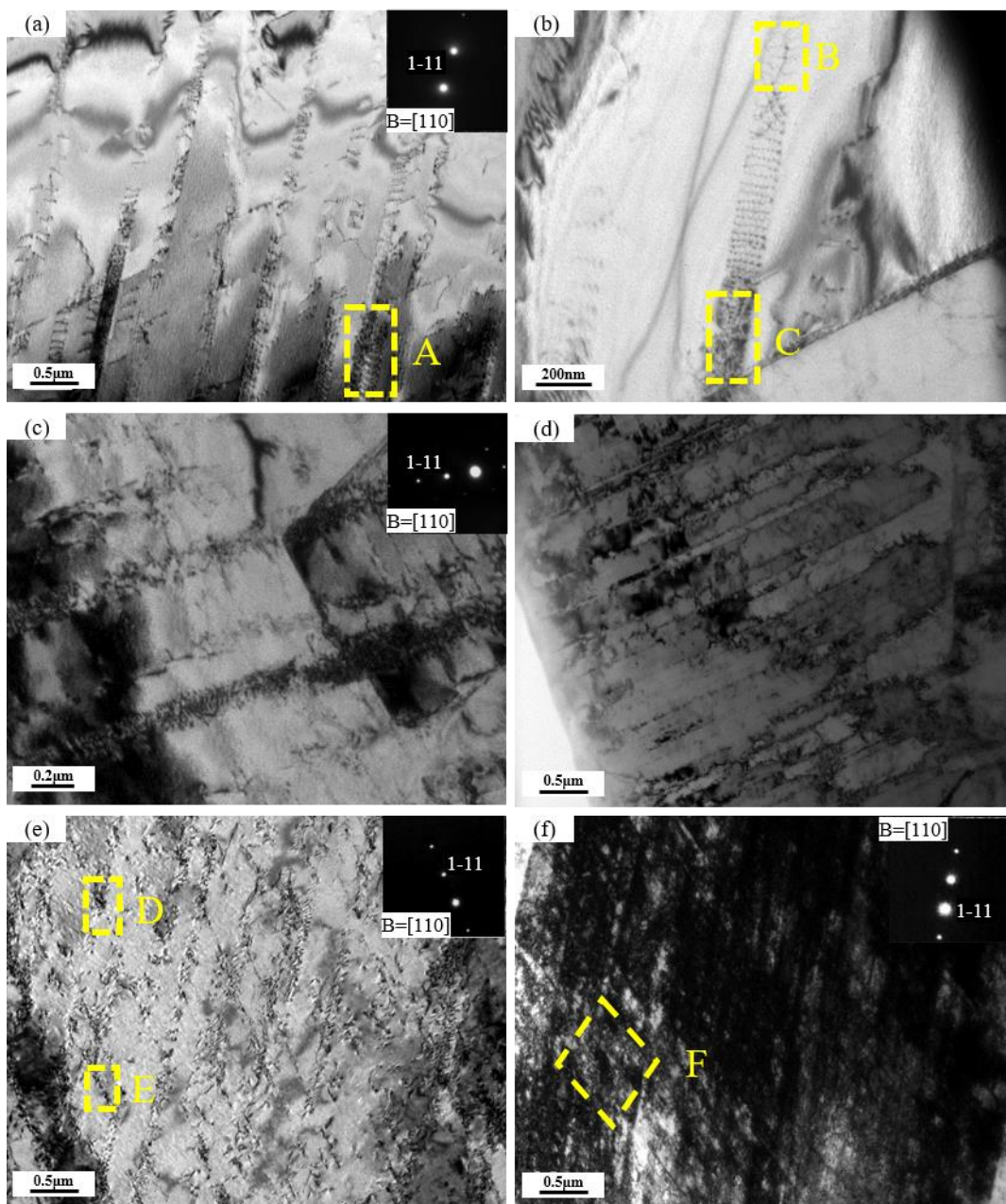


Figure 8. TEM images of different deformation of experimental steel. (a) 5%; (b) 5%; (c) 10%; (d) 10%; (e) 20%; and (f) 50%.

4. Conclusions

In this paper, the effect of annealing process parameters on the mechanical properties (tensile strength, elongation, product of strength and plasticity, and specific strength) of Fe-28.7Mn-10.2Al-1.06C highly specific strength steel was studied. Combined with metallographic structure, SEM morphology, XRD pattern, and TEM, the effects of annealing process on microstructure, grain size, and twinning of experimental steel were analyzed, and the deformation behavior of experimental steel under quasi-static tensile was analyzed. The final conclusions of this paper are as follows:

(1) Due to the addition of low-density elements such as Al and C, the density of the experimental steel was measured to be 6.59 g/cm^3 , which was 15.4% lower than that of pure iron.

(2) The microstructure of the experimental steel and the annealed steel at room temperature is single austenite phase. With the increase in annealing temperature, the grain

increases. A large number of annealing twins are distributed in the austenite matrix, and the twins run through the entire austenite grain.

(3) With the increase in annealing temperature, the yield strength and tensile strength of Fe-Mn-Al-C steel decrease, and the elongation increases. When the annealing temperature was 950 °C, the yield strength of the experimental steel was 619.2 MPa, the tensile strength was 977.2 MPa, the elongation was 56.1%, the product of strength and plasticity was 54.82 GPa%, and the specific strength was 1.48×10^5 N·m/kg, with the best comprehensive performance. Compared with 20Mn2CrNb high strength automobile steel with tensile strength of 905 MPa and density of 7.8 g/cm³, the specific strength of laboratory steel is increased by more than 20%.

(4) In the deformation process of experimental steel, the spacing of slip surface decreases and the dislocation density increases at low strain. At high strain, dislocation walls and micro-strip structures are formed, and austenite grains are segmented, which increases dislocation density and activates more secondary slip.

Author Contributions: Writing—Original, L.M.; Conceptualization, Z.T.; and Writing—Review and Editing, Z.Y.; G.G.; H.D.; and D.M. All authors have read and agreed to the published version of the manuscript.

Funding: The research was supported by the National Natural Science Foundation of China (Grant No. 51874088) and Fundamental Research Funds for the Central Universities (N2002015).

Data Availability Statement: The raw/processed data required to reproduce these findings cannot be shared at this time as the data also forms part of an ongoing study.

Acknowledgments: We are grateful to Devesh. Misra for the review/comments on the manuscript.

Conflicts of Interest: The authors declare no conflict of interest.

References

- Bouaziz, O.; Zurob, H.; Huang, M. Driving Force and Logic of Development of Advanced High Strength Steels for Automotive Applications. *Steel Res. Int.* **2013**, *84*, 937–947. [[CrossRef](#)]
- Zhao, J.; Jiang, Z. Thermomechanical processing of advanced high strength steels. *Prog. Mater. Sci.* **2018**, *94*, 174–242. [[CrossRef](#)]
- Kuziak, R.; Kawalla, R.; Waengler, S. Advanced high strength steels for automotive industry. *Arch. Civ. Mech. Eng.* **2008**, *8*, 103–117. [[CrossRef](#)]
- Chen, S.; Rana, R.; Haldar, A.; Ray, R. Current state of Fe-Mn-Al-C low density steels. *Prog. Mater. Sci.* **2017**, *89*, 345–391. [[CrossRef](#)]
- Park, K.-T.; Hwang, S.W.; Son, C.Y.; Lee, J.-K. Effects of Heat Treatment on Microstructure and Tensile Properties of a Fe-27Mn-12Al-0.8C Low-Density Steel. *JOM* **2014**, *66*, 1828–1836. [[CrossRef](#)]
- Zhang, J.; Hu, C.; Zhang, Y.; Li, J.; Song, C.; Zhai, Q. Microstructures, mechanical properties and deformation of near-rapidly solidified low-density Fe-20Mn-9Al-1.2C-xCr steels. *Mater. Des.* **2020**, *186*, 307. [[CrossRef](#)]
- Ren, P.; Chen, X.P.; Wang, C.Y.; Zhou, Y.X.; Cao, W.Q.; Liu, Q. Evolution of microstructure, texture and mechanical properties of Fe-30Mn-11Al-1.2C low-density steel during cold rolling. *Mater. Charact.* **2021**, *174*, 111013. [[CrossRef](#)]
- Gutierrez-Urrutia, I. Low Density Steels. *Ref. Modul. Mater. Sci. Mat. Eng.* **2022**, *2*, 106–114. [[CrossRef](#)]
- Piston, M.; Bartlett, L.; Limmer, K.R.; Field, D.M. Microstructural Influence on Mechanical Properties of a Lightweight Ultrahigh Strength Fe-18Mn-10Al-0.9C-5Ni (wt%) Steel. *Materials* **2020**, *10*, 1305. [[CrossRef](#)]
- Raabe, D.; Springer, H.; Gutierrez-Urrutia, I.; Roters, F.; Bausch, M.; Seol, J.-B.; Koyama, M.; Choi, P.-P.; Tsuzaki, K. Alloy Design, Combinatorial Synthesis, and Microstructure-Property Relations for Low-Density Fe-Mn-Al-C Austenitic Steels. *JOM* **2014**, *66*, 1845–1856. [[CrossRef](#)]
- Mondal, A.; Pilone, D.; Brotzu, A.; Felli, F. Effect of heat treatment on mechanical properties of FeMnAlC alloys. *Procedia Struct. Integr.* **2021**, *33*, 237–244. [[CrossRef](#)]
- Kim, M.S.; Kang, Y.B. Development of thermodynamic database for high Mn-high Al steels: Phase equilibria in the Fe-Mn-Al-C system by experiment and thermodynamic modeling. *Calphad* **2015**, *51*, 89–103. [[CrossRef](#)]
- Zhao, C.; Song, R.; Zhang, L.; Yang, F.; Kang, T. Effect of annealing temperature on the microstructure and tensile properties of Fe-10Mn-10Al-0.7C low-density steel. *Mater. Des.* **2016**, *91*, 348–360. [[CrossRef](#)]
- Yoo, J.D.; Si, W.H.; Park, K.T. Factors Influencing the Tensile Behavior Of A Fe-28Mn-9Al-0.8C Steel. *Mater. Sci. Eng. A* **2009**, *508*, 234–240. [[CrossRef](#)]
- Frommeyer, G.; Brück, U. Microstructures and mechanical properties of high-strength Fe-Mn-Al-C light-weight TRIPLEX steels. *Steel Res. Int.* **2006**, *77*, 627–633. [[CrossRef](#)]

16. Welsch, E.; Ponge, D.; Haghighat, S.M.H.; Sandlöbes, S.; Choi, P.; Herbig, M.; Zaeferrer, S.; Raabe, D. Strain hardening by dynamic slip band refinement in a high-Mn lightweight steel. *Acta Mater.* **2016**, *116*, 188–199. [[CrossRef](#)]
17. Sutou, Y.; Kamiya, N.; Umino, R.; Ohnuma, I.; Ishida, K. High-strength Fe–20Mn–Al–C-based Alloys with Low Density. *ISIJ Int.* **2010**, *50*, 893–899. [[CrossRef](#)]
18. Field, D.M.; Limmer, K.R.; Hornbuckle, B.C. On the Grain Growth Kinetics of a Low Density Steel. *Materials* **2019**, *9*, 997. [[CrossRef](#)]
19. Shaozun, L.; Yong, L.; Chunxu, W.; Shunzhe, H.; Shun, H.; Xianmin, L. Effect of Solution Treatment on Microstructure and Properties of Fe-Mn-Al-C Low Density Steel. *Heat Treat. Met.* **2015**, *40*, 5. [[CrossRef](#)]
20. Jian, C.; Fei, H.; Hanlin, D.; Guohui, Z.; Qiwei, C.; Guangping, C.; Zijian, W. Effect of heat treatment on microstructure and properties of ultra-high strength 20Mn2Cr automobile steel. *J. Mater. Heat Treat.* **2021**, *42*, 9.
21. Etienne, A.; Massardier-Jourdan, V.; Cazottes, S.; Garat, X.; Soler, M.; Zuazo, I.; Kleber, X. Ferrite Effects in Fe-Mn-Al-C Triplex Steels. *Metall. Mater. Trans. A* **2014**, *45*, 324–334. [[CrossRef](#)]
22. Shi, Y.; Zhang, Y.Y.; Liu, F.; Jin, X.M.; Guo, X.X. Research progress of face-centered cubic metal grain boundary engineering technology. *Hot Work. Process.* **2020**, *49*, 5. [[CrossRef](#)]
23. Castañeda, J.A.; Zambrano, O.A.; Alcázar, G.A.; Rodríguez, S.A.; Coronado, J.J. Stacking Fault Energy Determination in Fe-Mn-Al-C Austenitic Steels by X-ray Diffraction. *Metals* **2021**, *11*, 1701. [[CrossRef](#)]
24. Zhang, X.F.; Leng, D.P.; Zhang, L.; Zhenyi, H.; Guang, C. Effect of Al content on stacking fault energy and deformation twins of Fe-Mn-Al-C low density steel. *J. Mat. Heat Treat.* **2015**, *36*, 6.
25. Jin, J.E.; Lee, Y.K. Effects of Al on microstructure and tensile properties of C-bearing high Mn TWIP steel. *Acta Mater.* **2012**, *60*, 1680–1688. [[CrossRef](#)]
26. Song, W.; Ingendahl, T.; Bleck, W. Control of Strain Hardening Behavior in High-Mn Austenitic Steels. *Acta Metall. Sin.* **2014**, *27*, 546–556. [[CrossRef](#)]
27. Hua, D.; Dong, H.; Zhang, J.; Cai, Z.; Wu, Z.; Cai, M. Tensile deformation behavior analysis of low density Fe–18Mn–10Al–xC steels. *Mat. Sci. Eng. A* **2016**, *652*, 69–76. [[CrossRef](#)]
28. Huo, Y.-T.; He, Y.-L.; Zhu, N.-Q.; Ding, M.-L.; Liu, R.-D.; Zhang, Y. Deformation Mechanism Investigation on Low Density 18Mn Steels under Different Solid Solution Treatments. *Metals* **2021**, *11*, 1497. [[CrossRef](#)]
29. Pang, J.; Zhou, Z.; Zhao, Z.; Tang, D.; Liang, J.; He, Q. Tensile Behavior and Deformation Mechanism of Fe-Mn-Al-C Low Density Steel with High Strength and High Plasticity. *Metals* **2019**, *9*, 897. [[CrossRef](#)]